

Unstable density distribution associated with equatorial plasma bubble

E. A. Kherani, R. Bharuthram, S. Singh, G. S. Lakhina, and F. Carlos de Meneses

Citation: *Physics of Plasmas* **23**, 042901 (2016); doi: 10.1063/1.4945636

View online: <http://dx.doi.org/10.1063/1.4945636>

View Table of Contents: <http://scitation.aip.org/content/aip/journal/pop/23/4?ver=pdfcov>

Published by the [AIP Publishing](#)

Articles you may be interested in

[Effect of q-nonextensive parameter and saturation time on electron density steepening in electron-positron-ion plasmas](#)

Phys. Plasmas **22**, 112109 (2015); 10.1063/1.4935404

[Particle in cell simulations of Buneman instability of a current-driven plasma with q-nonextensive electron velocity distribution](#)

Phys. Plasmas **21**, 092307 (2014); 10.1063/1.4896243

[Multicomponent kinetic simulation of Bernstein–Greene–Kruskal modes associated with ion acoustic and dust-ion acoustic excitations in electron-ion and dusty plasmas](#)

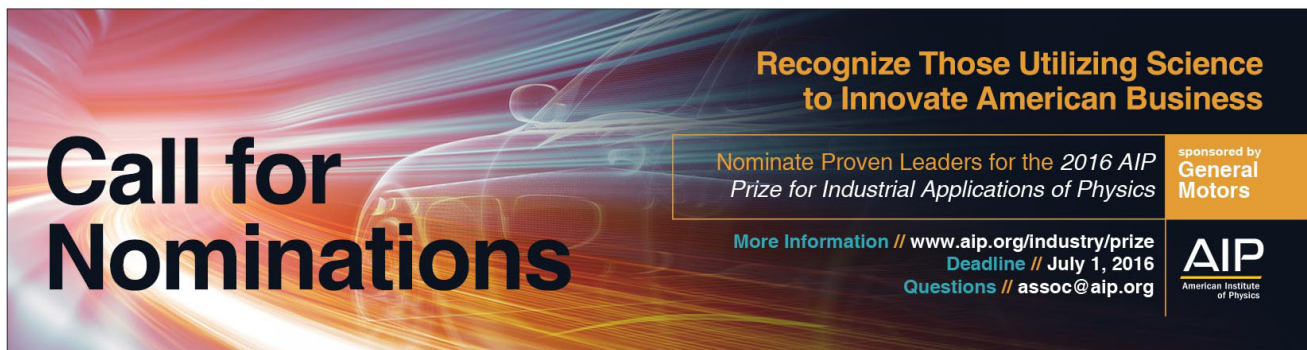
Phys. Plasmas **21**, 043701 (2014); 10.1063/1.4869730

[A multi-dimensional Vlasov-Fokker-Planck code for arbitrarily anisotropic high-energy-density plasmas](#)

Phys. Plasmas **20**, 056303 (2013); 10.1063/1.4801750

[Electron velocity distributions during beam–plasma interaction](#)

Phys. Plasmas **11**, 80 (2004); 10.1063/1.1631288



Call for Nominations

Recognize Those Utilizing Science to Innovate American Business

Nominate Proven Leaders for the 2016 AIP Prize for Industrial Applications of Physics

More Information // www.aip.org/industry/prize
Deadline // July 1, 2016
Questions // assoc@aip.org

sponsored by General Motors

AIP
American Institute of Physics

Unstable density distribution associated with equatorial plasma bubble

E. A. Kherani,^{1,a)} R. Bharuthram,² S. Singh,^{3,2} G. S. Lakhina,^{3,2} and F. Carlos de Meneses¹

¹*Instituto Nacional de Pesquisas Espaciais (INPE), Brazil*

²*University of Western Cape, Bellville, South Africa*

³*Indian Institute of Geomagnetism, Mumbai, India*

(Received 20 January 2016; accepted 23 March 2016; published online 11 April 2016)

In this work, we present a simulation study of equatorial plasma bubble (EPB) in the evening time ionosphere. The fluid simulation is performed with a high grid resolution, enabling us to probe the steepened updrafting density structures inside EPB. Inside the density depletion that eventually evolves as EPB, both density and updraft are functions of space from which the density as implicit function of updraft velocity or the density distribution function is constructed. In the present study, this distribution function and the corresponding probability distribution function are found to evolve from Maxwellian to non-Maxwellian as the initial small depletion grows to EPB. This non-Maxwellian distribution is of a gentle-bump type, in confirmation with the recently reported distribution within EPB from space-borne measurements that offer favorable condition for small scale kinetic instabilities. © 2016 AIP Publishing LLC. [<http://dx.doi.org/10.1063/1.4945636>]

I. INTRODUCTION

Plasma instabilities play an important role in determining the state of equatorial ionosphere. The evening-time F region of ionosphere becomes unstable under collisional interchange instability (CII) mechanism, which is the generic name for $E \times B$ and Rayleigh-Taylor instabilities.¹ Non-linear development of CII in the F region of ionosphere triggers the equatorial plasma bubble (EPB) characterized by updrafting high degree of plasma density depletion.²⁻⁴ Moreover, inside EPB, plasma mainly drifts vertical, by leading to the establishment of an anisotropic environment composed of steep density structures.⁵

Numerous observations show that EPBs are large scale density depletion of scale size $\sim 1-100$ km. More strikingly, within the large scale EPB, small scale (\sim meters to centimeters) size irregularities (SSIs) are found to be present.⁶ The underlying mechanisms for the generation of SSI remain unresolved though, it is understood that the sharp density gradients within EPB can trigger the small scale instabilities that gives rise to SSI.⁷ The widely examined small scale instabilities are the drift and lower hybrid drift wave instabilities which are shown to satisfy the growth conditions inside EPB.⁸⁻¹⁰

An important input to these analyses is the Probability Distribution Function (PDF) which is often considered as Maxwellian or drifting-Maxwellian.¹¹ However, since SSIs are developed within the unstable EPB that is characterized by large anisotropic kinetic energy distribution, the PDF is likely to acquire a non-Maxwellian nature. In fact, the PDF within EPB as deduced from the rocket measurement is found to be non-Maxwellian of gentle-bump type, having a bump at higher energy tail.¹² The origin of such PDF within EPB remains unclear. Therefore, it is desirable to simulate the density distribution function (DDF) and the corresponding PDF within the EPB from simulation of CII whose knowledge may facilitate further understanding of the

generation mechanism of SSI. In this study, we perform the simulation of EPB, construct the DDF and the PDF, and examine possible growth condition for the drift wave offered by the non-Maxwellian nature of PDF.

II. SIMULATION MODEL

In the present study, we employ the two dimensional (longitude-altitude) version of three-dimensional (longitude-altitude-latitude) simulation model of CII/EPB developed by Kherani *et al.*,¹³ by fixing latitude = 0° corresponding to the geomagnetic equator. The model solves the following hydro-magnetic equations in the ionosphere:

$$\frac{\partial \vec{v}_s}{\partial t} = \vec{g} + \frac{q_s}{m_s} (\vec{E} + \vec{v}_s \times \vec{B}) - \nu_s \vec{v}_s, \quad (1)$$

(s = ions (i)/electrons (e)),

$$\frac{\partial n_s}{\partial t} + \nabla \cdot (n_s \vec{v}_s) = -R_e n_s, \quad (n_i = n_e = n), \quad (2)$$

$$\vec{J} = \underline{\sigma} \cdot \vec{E}, \quad (3)$$

$$\nabla \cdot \vec{J} = 0 \quad \Rightarrow \quad \nabla \cdot (\underline{\sigma} \cdot \vec{E}) = 0 \quad \Rightarrow \quad \nabla \cdot \vec{E} = -\sigma^{-1} (\vec{E} \cdot \nabla \underline{\sigma})$$

$$\vec{E} = \vec{E}_o - \nabla \phi \quad (4)$$

Here, \vec{g} , \vec{B}_o , and ν_s are the gravitational acceleration, Earth's magnetic field, and the collision frequency, and R_e is the recombination rate as described by Kherani *et al.*¹⁴ Equations (1)–(4) form a closed set of equations to study the temporal and spatial evolutions of ionospheric number density (n), conductivity ($\underline{\sigma}$), velocities ($\vec{v}_{i,e}$) of ions/electrons, electrostatic potential (ϕ), and electric field (\vec{E}). At $t = 0$, the ambient density (n_o) profile is considered the same as chosen by Kherani *et al.*¹⁴ while the ambient vertical drift ($v_o = E_o/B_o$) with a value of 40 m/s is considered for simplicity.

Equations (1)–(4) are solved numerically using a finite-difference method and the implicit Crank-Nicholson scheme is employed to perform the time integration, leading to a

^{a)}esfhan.kherani@inpe.br

matrix equation that is subsequently solved by the Successive-Over-Relaxation method.¹⁴ The simulation domain occupies a 2D Cartesian plane corresponding to the equatorial plane perpendicular to the Earth's magnetic field that consists of longitude (x) and altitude (y). The domain covers 300–500 km in altitude and -20 to $+20$ km in longitude with equal grid resolutions $\Delta x = \Delta y = 500$ m. At $t = 0$, a sinusoidal density perturbation (δn) with 1% amplitude with respect to the ambient density, and wavelength of 20 km, is given along the longitude such that $n = n_o + \delta n$.

III. RESULTS AND DISCUSSION

In Figures 1–3, the simulation results are presented. In Figure 1, the left panels show the longitude-altitude distribution of (n , v), in the form of iso-density contours (IDCs) and iso-velocity contours (IVCs), at three chosen times $t = 0$, 850, and 1200 s. Here, $v = v_{iy}$ is the ion updraft inside the EPB. Since both n and v are explicit function of space at given time, a DDF can be constructed by considering n as an implicit function of v . Such DDF is constructed by adding all densities in each 10 m/s window of -10 – 400 m/s updraft range that is encountered within the narrow-middle part of the EPB. The right panels in Figure 1 show DDF corresponding to the three chosen times. In Figure 2, IDCs/IVCs in the left panel and DDF in the right panel are shown at $t = 1350$ s, which represents the final stage of evolution of CII.

In the present study, the linear growth time of CII, $\tau = \frac{L}{(v_o + g/v_i)}$, varies between 300 and 700 s, as the scale

height (L) varies with the altitude. Therefore, the initial perturbation is expected to evolve nonlinearly during this time. In Figures 1 and 2, we note that the initial 1% density depletion evolves as updrafted EPB within 1200 s under the action of CII. (Here, EPB is defined as highly depleted region that drifts upward with $v \geq 2v_o \sim 80$ m/s.) The constructed DDF reveals the following characteristics:

1. During the initial linear phase ($0 \leq t \ll 850$) seconds of instability evolution, DDF is Maxwellian in nature.
2. During the non-linear phase ($850 \leq t \leq 1350$) seconds when updraft becomes larger than twice the ambient drift, DDF turns into non-Maxwellian acquiring extended tail at higher v representing the development of EPB.
3. The non-Maxwellian DDF is of the gentle-bump type, consisting of multiple bumps or Doppler pulses whose amplitudes gradually decrease (more depletion) with increasing v .
4. At $t = 1350$ s, a gentle-bump is developed at $100 \leq v \leq 150$ m/s.
5. This bump corresponds to moderate depletion as noted from Figure 2.

From DDF, the PDF can be constructed using the following definition:

$$f = \frac{\partial n}{\partial v}. \quad (5)$$

In Figure 3, the DDF and the corresponding PDF at $t = 1350$ s are plotted. We note that the PDF follows DDF

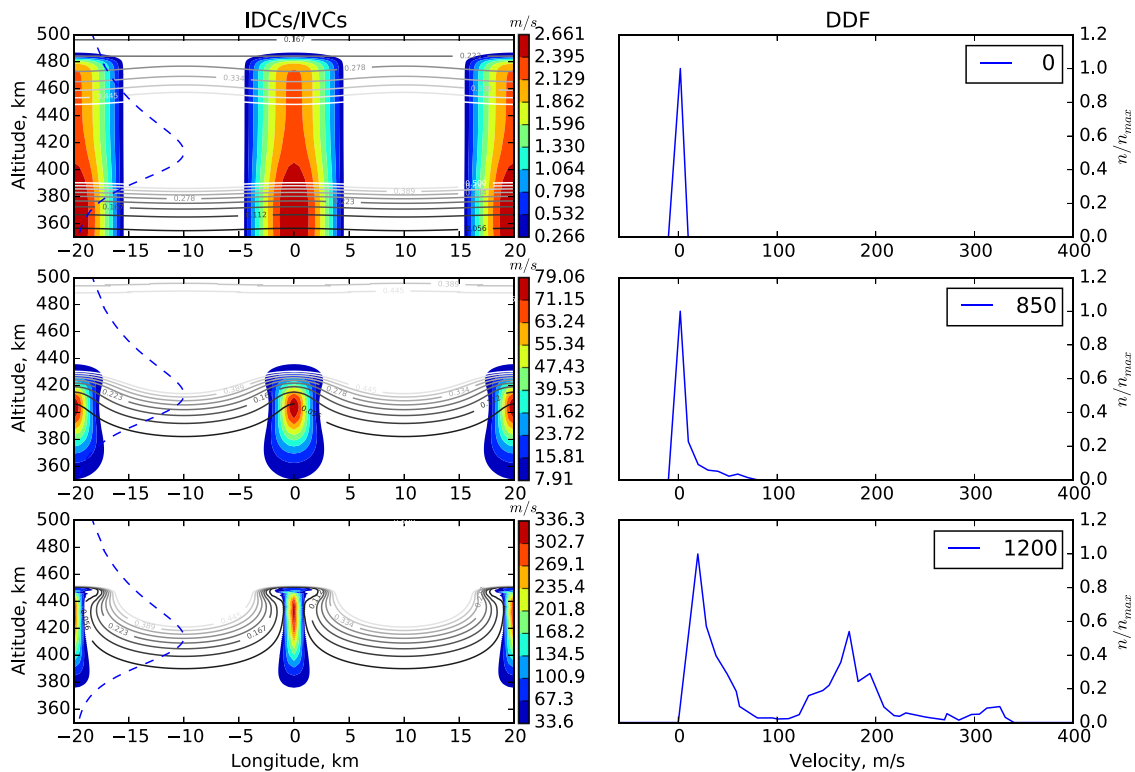


FIG. 1. Evolution of CII: Left-panels show the longitude-altitude distribution of (n , v), in the form of IDCs and IVCs, at three chosen times, $t = 0$, 850, and 1200 s. IDCs and IVCs are represented by contours and color-pixmap. In the right-panel, the corresponding DDFs are plotted. The DDF is constructed by counting the number density encountered within a narrow-middle part of EPB in each 10 m/s window of v ranging between -10 and 400 m/s. The DDF is normalized to the maximum density (n_{\max}) which is 10^{14} , 5×10^{13} , 10^{12} m^{-3} at three chosen times. In the left panels, the dashed blue curve represents the ionospheric number density and $t = 0$ s.

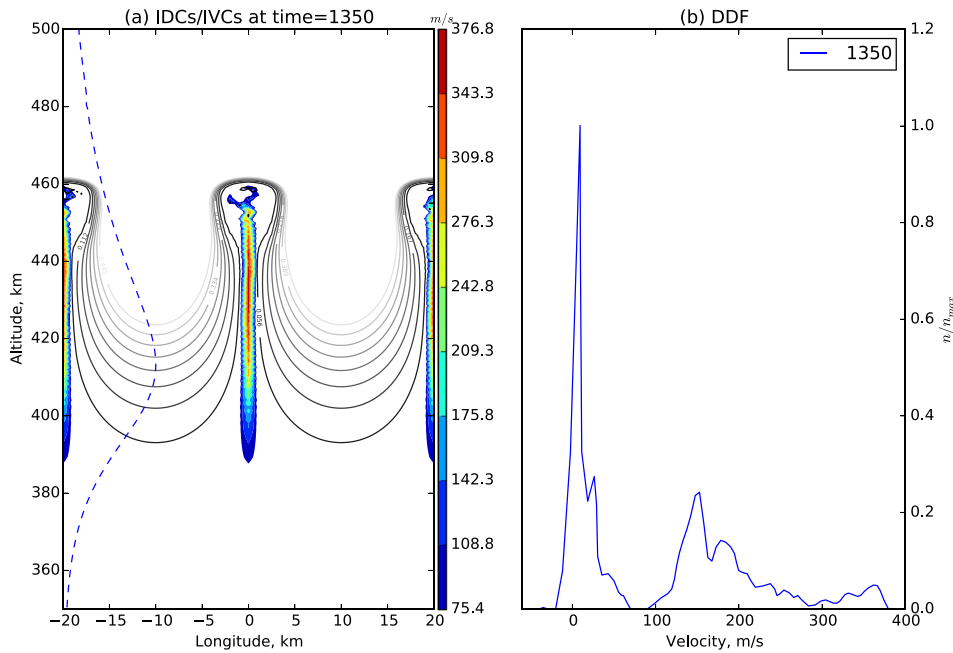


FIG. 2. The left and right panels show IDCs/IVCs and corresponding DDF at $t = 1350$ s which is the final stage of evolution of CII.

revealing a non-Maxwellian nature with a gentle bump at $v \sim 100\text{--}150$ m/s. This Doppler pulse corresponds to an EPB which is streaming through the ambient ionosphere with the bulk updraft $v = \frac{\partial E}{\partial v} \sim 100 - 150$ m/s due to the CII. We also note that within the EPB, the density depletion has large probability to ensemble around this bulk updraft, though it also has secondary maxima at higher updrafts. Also, the large probability is noted at $v \sim 30$ m/s, but this does not belong to the EPB due to its updraft comparable to the ambient and is associated with the bulk ambient motion.

Such gentle-bump PDF associated with EPB has been reported from the rocket measurements¹² though its origin had remained unclear. In the present study, we simulate it and show that they are caused by the CII dynamics. The gentle bump arises due to the fact that the large part of EPB tends to ensemble around sufficiently large Doppler range that still has sufficient density though highly depleted than the ambient density. Outside this Doppler range, either

depletion has updraft too small to be considered as EPB or it has too large updraft with insignificant density.

A. Possible role of gentle-bump to destabilize the drift wave and SSI

The broad gentle-bump in Figure 3 offers stable ($\frac{\partial f}{\partial v} < 0$) and unstable ($\frac{\partial f}{\partial v} > 0$) conditions and the small scale kinetic plasma waves with phase velocities (v_{ph}) in the region of positive $\frac{\partial f}{\partial v} > 0$ can become unstable.¹⁵ Therefore, the kinetic plasma waves with $v_{ph} \sim 100\text{--}150$ m/s are likely to become unstable in the presence of such gentle-bump PDF. In this context, we examine the drift wave which is argued as the most favorable small scale wave to be excited within EPB.^{9,10} The kinetic drift wave phase velocity is given by the following expression:⁹

$$v_{ph} = \frac{v_{th}^2}{\Omega_i L} \hat{b} \times \hat{\nabla} n, \quad (6)$$

where v_{th} , Ω_i , and L are the ion thermal speed, gyro-frequency, and the density gradient scale within the EPB, respectively. For the typical F region parameters, $600 \leq v_{th} \leq 10^3$ m/s and $10^2 \leq \Omega_i \leq 2 \times 10^2 \text{ s}^{-1}$. The density gradient scale length (L) depends on the state of EPB and for a well developed EPB, it can vary between 50 and 10^3 m, as noted from the rocket observations.⁸ Therefore, v_{ph} is bounded between $2 \leq v_{ph} \leq 200$ m/s. Therefore, for the typical F region parameters and observed L values, v_{ph} of drift wave is likely to encounter the unstable condition offered by the gentle-bump PDF derived in the present study, leading to the growth of drift wave which can subsequently excite the SSI.

In the previous studies of SSI within EPB, drifting-Maxwellian (f_{dm}) kind of PDFs were considered in which both ions and electron are drifting with same diamagnetic drift but in the opposite direction.¹¹ In the present study, the derived PDF is of gentle-bump type in which the whole

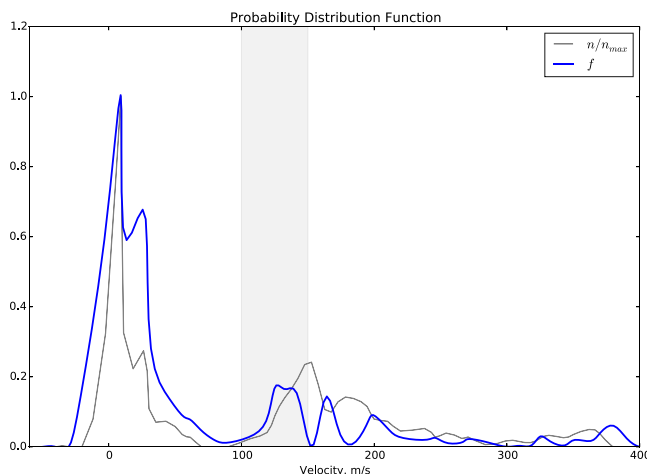


FIG. 3. PDF: The blue curve represents the PDF constructed from the DDF (gray curve) at $t = 1350$ s. The shaded rectangle represents the broad gentle-bump of interest.

plasma within EPB is drifting with the bulk updraft $\sim 100\text{--}150\text{ m/s}$ arising from the nonlinear dynamics of CII and not due to the diamagnetic drift. Another noteworthy difference is that the gentle-bump in Figure 3 offers much larger $\frac{\partial f}{\partial v} \sim \frac{1}{50}$ than the drifting-Maxwellian which has $\frac{\partial f}{\partial v} \propto \frac{1}{v_{th}} \sim \frac{1}{10^3}$ and since the growth rate $\gamma \propto \frac{\partial f}{\partial v}$, we expect the growth rate with the derived PDF to be much larger than its value with the drifting-Maxwellian. To elaborate this aspect in more detail, we examine the following growth rate (γ_{dm}) expression of the drift wave instability for the drifting-Maxwellian PDF (f_{dm}), as given by Huba and Ossakow¹¹

$$\gamma_{dm} = \omega \frac{v_{di}}{v_{th}} \frac{k^2 \rho_s^2}{(1 + k^2 \rho_s^2)^2}. \quad (7)$$

Here, $v_{di} = v_{ph} \frac{\omega}{k}$ is the phase velocity of the wave and ρ_s is the ion Larmor radius. On the other hand, for the derived gentle-bump PDF (f) in the present study, the growth rate (γ_{gb}) can be written as follows:

$$\gamma_{gb} = \alpha \omega \frac{v_{di}}{\Delta v} \frac{k^2 \rho_s^2}{(1 + k^2 \rho_s^2)^2}, \quad (8)$$

where Δv is the Doppler dispersion of broad gentle-bump in Figure 3, which is of order of $\sim 50\text{ m/s}$ and $\alpha = \frac{f}{f_{dm}} \leq 1$ is the relative population of two PDFs. Therefore, the ratio of two growth rate can be obtained as follows:

$$\frac{\gamma_{gb}}{\gamma_{dm}} = \alpha \frac{v_{th}}{\Delta v}.$$

In Figure 3, we note that the broad gentle-bump has $f \sim 0.15$ while the drifting-Maxwellian, in general, can have a population in the range of $0.5 \leq f_{dm} \leq 1$, leading to $0.15 \leq \alpha \leq 0.3$. Considering $600 \leq v_{th} \leq 10^3\text{ m/s}$, we can have following bounds for the ratio:

$$1.8 \leq \frac{\gamma_{gb}}{\gamma_{dm}} \leq 6.$$

Therefore, in general, the gentle-bump PDF derived in the present study offers larger growth rate of drift wave instability than that offered by a drifting-Maxwellian PDF.

As discussed by Huba and Ossakow (1979),¹⁰ the drift wave instability could be heavily damped by ion viscosity with the following viscous damping rate:

$$\gamma_{damp}^{dm} = \frac{3(\pi + 1)}{4\sqrt{2}} \nu_{ii} k^2 \rho_s^2,$$

where ν_{ii} is the ion-ion collision frequency responsible for the viscosity and superscript “dm” stands for the drifting-Maxwellian. This expression was derived for the drifting-Maxwellian distribution function. In our study, for the gentle-bump distribution, we may write this expression as follows:

$$\gamma_{damp}^{gb} = \alpha \frac{3(\pi + 1)}{4\sqrt{2}} \nu_{ii} k^2 \rho_s^2 = \alpha \gamma_{damp}^{dm},$$

where $\alpha = f/f_{dm} \leq 1$ is the relative population, as defined in Equation (8) and superscript “gb” stands for the gentle-bump

distribution. Since $0.15 \leq \alpha \leq 0.3$, therefore, we expect the viscous damping rate to be smaller for the gentle-bump distribution in comparison to the drifting Maxwellian distribution. This is because the f in Figure 3 has lesser density population in the unstable gentle-bump than the drifting Maxwellian, leading to less collision and therefore less viscous damping.

The drift wave instability is expected to be excited inside the EPB in the region with the largest density gradient. To examine this aspect, we plot the distribution of horizontal and vertical density gradients, ∂_h and ∂_v in Figure 4. These gradients are defined as follows:

$$\partial_h = \frac{1}{n} \frac{\partial n}{\partial x}, \quad \partial_v = \frac{1}{n} \frac{\partial n}{\partial y}.$$

From this figure, we note that both ∂_h and ∂_v become largest in $100\text{--}200\text{ m/s}$, i.e., the broad gentle-bump under consideration offers the largest density gradients. In fact, both ∂_h and ∂_v tend to acquire peaks in all those velocity ranges where the distribution has the gentle-bump characteristics. It is interesting to note that ∂_h also becomes large around $v = 0$, i.e., across the wall of the bubble as expected, however ∂_v is small at this location. The gentle bump residing in $100\text{--}200\text{ m/s}$ velocity range offers unique scenario where both ∂_h and ∂_v are largest, which should be more suitable for the growth of drift wave instability.

IV. SUMMARY

In this study, we have presented a simulation study of EPB in the evening-time equatorial ionosphere and deduced the density distribution function and associated probability distribution functions (f). They are found to evolve from an initial Maxwellian to a Non-Maxwellian of gentle-bump type as the initial small depletion grows to EPB under the action of CII. This non-Maxwellian f consists of a broad bump or Doppler pulse located within the $100\text{--}150\text{ m/s}$ velocity range, arising from the bulk updraft of EPB relative to the ambient ionosphere, caused by the CII. It is shown that for typical F region parameters and the observed density

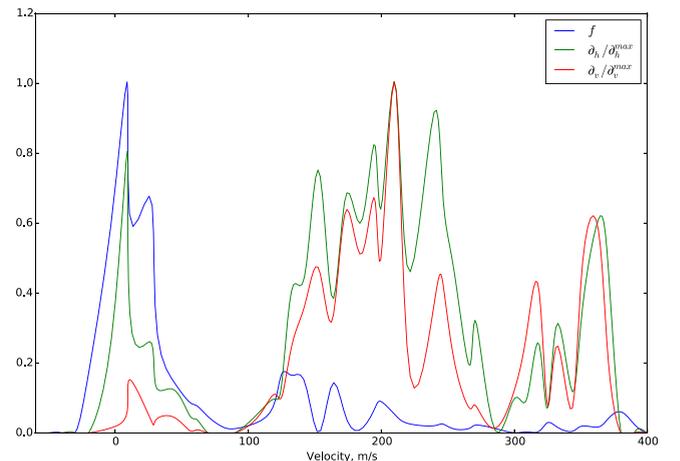


FIG. 4. The density gradient distributions at $t = 1350\text{ s}$: The green and red curves represent the distributions of horizontal and vertical density gradients, ∂_h and ∂_v . They are normalized to their corresponding maximum values. For comparison, the PDF (f) is also plotted as the blue curve.

gradient scale length between 50 and 10^3 m, the associated drift wave can acquire the phase velocity satisfying the unstable criteria $\frac{\partial f}{\partial v} > 0$, suggesting their likely destabilization. It is argued that this non-Maxwellian f offers larger $\frac{\partial f}{\partial v}$ in comparison to the drifting-Maxwellian considered in the previous studies of drift wave instability within EPB and, as a result, is likely to accelerate the instability growth by factor of 2–6. The present study offers an alternative distribution function to be examined in the context of small scale plasma waves such as the drift and lower hybrid waves which until now have been examined with only the drifting-Maxwellian distribution function.

ACKNOWLEDGMENTS

This work was carried out with the financial support from FAPESP-Brasil (2011/21903-3) and NRF-South Africa (92058). G.S.L. is thankful to the National Academy of Sciences, India, for the support under the NASI Senior Scientist Platinum Jubilee Fellowship Scheme. F. C. de Meneses acknowledges the support given by CNPq under the grant number 312704/2015-1.

- ¹S. Zargham and C. E. Seyler, "Collisional interchange instability: 1. Numerical simulations of intermediate-scale irregularities," *J. Geophys. Res.* **92**(A9), 10073–10088, doi:10.1029/JA092iA09p10073 (1987).
- ²C.-S. Huang, M. C. Kelley, and D. L. Hysell, "Nonlinear Rayleigh-Taylor instabilities, atmospheric gravity waves and equatorial spread F," *J. Geophys. Res.* **98**(A9), 15631–15642, doi:10.1029/93JA00762 (1993).
- ³M. J. Keskinen, S. L. Ossakow, and B. G. Fejer, "Three-dimensional nonlinear evolution of equatorial ionospheric spread-F bubbles," *Geophys. Res. Lett.* **30**(16), 1855, doi:10.1029/2003GL017418 (2003).

- ⁴J. D. Huba and G. Joyce, "Equatorial spread F modeling: Multiple bifurcated structures, secondary instabilities, large density "bite-outs," and supersonic flows," *Geophys. Res. Lett.* **34**, L07105, doi:10.1029/2006GL028519 (2007).
- ⁵R. Sekar and E. A. Kherani, "The method of characteristic for nonlinear generalized Rayleigh-Taylor instability associated with equatorial spread F: An analytical approach," *Phys. Plasmas* **9**, 2754 (2002).
- ⁶B. B. Balsley, G. Haerendel, and R. A. Greenwald, "Equatorial spread F: Recent observations and a new interpretation," *J. Geophys. Res.* **77**(28), 5625–5628, doi:10.1029/JA077i028p05625 (1972).
- ⁷J. LaBelle, M. C. Kelley, and C. E. Seyler, "An analysis of the role of drift waves in equatorial spread F," *J. Geophys. Res.* **91**(A5), 5513–5525, doi:10.1029/JA091iA05p05513 (1986).
- ⁸E. Costa and M. C. Kelley, "On the role of steepened structures and drift waves in equatorial spread F," *J. Geophys. Res.* **83**, 4359, doi:10.1029/JA083iA09p04359 (1978a).
- ⁹E. Costa and M. C. Kelley, "Linear theory for collisionless drift waves with wavelengths near the ion gyroradius," *J. Geophys. Res.* **83**, 4365–4368, doi:10.1029/JA083iA09p04365 (1978b).
- ¹⁰J. Huba and S. Ossakow, "On the generation of 3-m irregularities during equatorial spread F by low-frequency drift waves," *J. Geophys. Res.* **84**(A11), 6697–6700, doi:10.1029/JA084iA11p06697 (1979).
- ¹¹J. Huba and S. Ossakow, "Physical mechanism of the lower-hybrid-drift instability in a collisional plasma," *J. Atmos. Sol. Terr. Phys.* **43**, 775–778 (1981).
- ¹²H. Thiemann, J. J. Sojka, J. J. Eccles, P. B. Rao, P. V. S. Rama Rao, R. Sridharan, and G. S. Lakhina, "Indo-German low-latitude project DEOS: Plasma bubbles in the post sunset and nighttime sector," *Adv. Space Res.* **27**, 1065–1069 (2001).
- ¹³E. A. Kherani and A. K. Patra, "Fringe field dynamics over equatorial and low-latitude ionosphere: A three-dimensional perspective," *J. Geophys. Res. Space Phys.* **120**, 6941–6947 (2015).
- ¹⁴E. A. Kherani, E. R. de Paula, and F. C. P. Bertoni, "Effects of the fringe field of Rayleigh-Taylor instability in the equatorial E and valley regions," *J. Geophys. Res.* **109**, A12310, doi:10.1029/2003JA010364 (2004).
- ¹⁵S. Ichimaru, *Statistical Plasma Physics: Basic Principles* (Westview Press, 2004).